



# Influence of geometry on galvanic corrosion of AZ91D coupled to steel

Jimmy X. Jia, Guangling Song, Andrej Atrens \*

*CRC for Cast Metals Manufacturing (CAST), Division of Materials Engineering, School of Engineering, The University of Queensland, St. Lucia, Brisbane, Qld 4072, Australia*

Received 29 November 2004; accepted 9 August 2005

Available online 10 October 2005

---

## Abstract

The influence of geometric factors on the galvanic current density distribution for AZ91D coupled to steel was investigated using experimental measurements and a BEM model. The geometric factors were area ratio of anode/cathode, insulation distance between anode and cathode, depth of solution film covering the galvanic couple and the manner of interaction caused by two independent interacting galvanic couples. The galvanic current density distribution calculated from the BEM model was in good agreement with the experimental measurements. The galvanic current density distribution caused by the interaction of two independent galvanic couples can be reasonably predicted as the linear addition of the galvanic current density caused by each individual galvanic couple. © 2005 Elsevier Ltd. All rights reserved.

*Keywords:* A. Magnesium alloys; B. Boundary element method; C. Galvanic corrosion

---

## 1. Introduction

Magnesium is the most active structural metal and thus could suffer serious galvanic corrosion when in contact with any other metal. Galvanic corrosion is a major concern for magnesium in industrial design and material selection [1–3]. Therefore, the study of galvanic corrosion has become increasingly important with the rapid increase of magnesium usage in applications in the auto and aerospace industries [4,5].

---

\* Corresponding author. Tel.: +61 7 3365 3738; fax: +61 7 3365 3888.  
E-mail address: [a.atrens@minmet.uq.edu.au](mailto:a.atrens@minmet.uq.edu.au) (A. Atrens).

The galvanic cell geometry determines the galvanic current and thus significantly influences the galvanic corrosion behaviour. Geometrical factors include the anode/cathode area ratio, the insulation distance ( $s$ ) between the anode and cathode, electrolyte film depth ( $d$ ) and the shapes of the anode and cathode [3,6]. In practice, the geometrical shape of mechanical components can take various forms. Insulation spacers can also be used between two components made from different metals. The thickness of these spacers can be varied to vary the insulation distance between the anode and cathode. Additionally, the solution film depth can be different. Furthermore, there can be more than one galvanic couple such as many steel fasteners for one magnesium part, and there can be an interaction or superimposition of the current caused by each galvanic couple. Waber [7] studied the effect of the galvanic cell size in galvanic corrosion theoretically in 1956 and indicated that the galvanic current distribution can be influenced by the area ratio of the anode/cathode and the Wagner parameter. But his mathematical model was subjected to the condition that the polarization parameter was equal to the cathodic value. In practice, this is not true for a variety of material arrangements. There was also another problem that “the question of distribution of current is too difficult to present adequately since there was an interplay between the cell dimension and the Wagner parameter”. Furthermore, there was no experimental comparison with the theoretical model.

Recently, Song et al. [3] carried out a study of the galvanic corrosion of magnesium using a galvanic corrosion assembly (GCA) and systematically investigated the influence of cathode materials, the distance between anode and cathode and the anode/cathode area ratio. This study identified important effects such as the “alkalization”, “passivation”, “poisoning” and “short-cut” effects as well as the effectiveness of an insulating spacer in reducing galvanic corrosion. This laid a solid foundation for further studies on the galvanic corrosion of magnesium alloys. However, the results and theoretical conclusions of Song et al. were mainly qualitative. It is important to quantify these findings.

Studies by Astley [8,9], Fu [10], Adey and Niku [11] and Kasper and Valeriote [12] have indicated that numerical methods are promising for studying galvanic corrosion, and in particular for predicting the galvanic current density distribution. With the development of computer technology, a boundary element method (BEM) program BEASY has become widely used to study galvanic corrosion [13]. Our previous study showed that the BEASY program calculated current density values consistent with the theoretical expectations for the case of both linear and non-linear polarization curves as boundary conditions [14]. Our subsequent study [15] of galvanic corrosion of magnesium coupled to steel in 5% NaCl solution, corrosive water and auto coolant showed good agreement between the BEASY calculations and experimental measurement provided that an adequate boundary condition was used. Subsequently, we have examined the galvanic corrosion of magnesium coupled to a steel fastener [16]. The total corrosion rate was measured as a function of distance from the interface of the magnesium in the form of a sheet containing a mild steel circular insert (5–30 mm in diameter). The measured total corrosion rate was interpreted as due to galvanic corrosion plus self-corrosion. For a typical case, the self-corrosion was estimated [15] to be  $\sim 230$  mm/y for an area surrounding the interface and to a distance of about 1 cm from the interface.

The present study investigated the influence of geometry on the galvanic current density distribution of magnesium in contact to steel in NaCl solution using experimental measurements and the boundary element method (BEM). The approach was as follows. The research aim was to investigate an idealized one-dimension galvanic couple as

illustrated in Fig. 1(a). The first task was to design an experimental approach to enable experimental measurement of the current density distribution in such an idealized galvanic couple. The approach was to use a galvanic corrosion assembly (GCA) as used in our prior study [15] and as shown schematically in section in Fig. 1(b). Details are given in Section 2. A BEM model was set up using the BEASY program. The BEM model calculations were compared with the experimental measurements. The aim was to further evaluate the BEASY program for various geometric galvanic cells and to investigate the potential challenges of using BEASY to simulate galvanic corrosion of magnesium for various area ratios of anode/cathode, solution film depth and insulation distance.

Furthermore, there are situations where there are a number of fasteners, such as when there are a number of steel bolts for a magnesium component. This paper includes an investigation into the interaction of two galvanic couples. The approach was to build

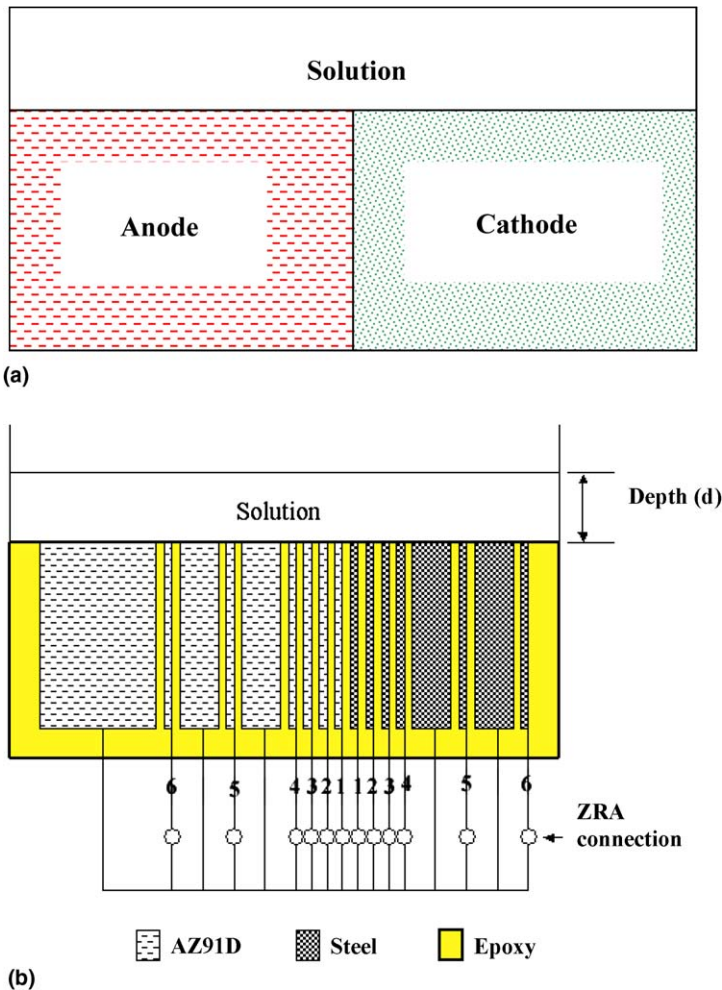


Fig. 1. (a) Schematic of idealised one-dimension galvanic couple. (b) Section through multi-electrode Mg–steel galvanic corrosion assembly (GCA).

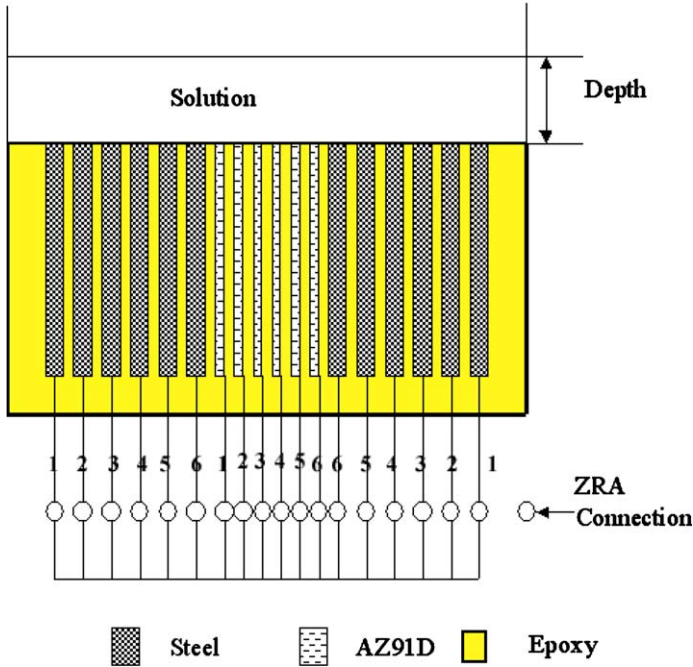


Fig. 2. Section through galvanic interaction assembly (GIA).

on our experience with the GCA [15] to design an experiment approach that would allow measurement of the current density distribution for the case of the interaction of two idealized 1D galvanic couples. The galvanic interaction assembly (GIA) is shown schematically in section in Fig. 2, and details are provided in Section 2. Again the experimental measurements were compared with a BEM model established using the BEASY program.

This research could provide helpful information for magnesium structure design and optimization in the auto and the aerospace industry.

## 2. Experimental procedure

### 2.1. Galvanic corrosion (1D) assembly

The galvanic corrosion assembly (GCA) was the same as in our previous study [15] and is shown schematically in section in Fig. 1(b). The top surface of the GCA models a galvanic couple of AZ91D–steel exposed to the solution. The AZ91D is on the left hand side whilst the steel is on the right hand side. Electrical connections through the bottom of the GCA allow measurement of the galvanic current density distribution for the AZ91D–steel galvanic couple. AZ91D ingot and mild steel were the materials. The magnesium alloy AZ91D was chosen because it is the most widely used magnesium alloy. AZ91D contains about 9% aluminium and less than 1% zinc. Mild steel is the most widely used metal in industry.

Metal plates (of AZ91D and steel) were molded in epoxy as shown in Fig. 1, with the cross-sectional area of the top of each plate exposed to the solution. The molding of the

plates into the GCA was such that there was no electrical contact between each plate through the epoxy (which is a good insulator). Electrical contact could be made to each plate via a lead through the bottom of the GCA through the epoxy. The GCA was equivalent to a galvanic couple of AZ91D coupled to steel when the top surface of the GCA was exposed to a solution and electrical contact was made between all the plates as shown in Fig. 1(b). Moreover, the current in each plate could be individually measured by the use of a zero resistance ammeter (ZRA) in the electrical circuit as shown in Fig. 1(b) (and the current density for each plate could be calculated by dividing the measured current by the area of the plate exposed to the solution). This allowed measurement of the current density distribution across the AZ91D–steel galvanic couple.

A zero insulating distance between adjacent plates would be preferable, but an insulation space of 0.5 mm was the smallest distance found to be practical. The dimension of the assembly into the plane of the figure was large compared with the thickness of each plate, so that the assembly can be considered to be close to an ideal one-dimension galvanic couple of AZ91D in contact with steel.

A 12 channel ZRA was available. This allowed 12 simultaneous measurements, and the standard configuration adopted was that shown in Fig. 1(b). Twelve plates of identical size were used for the galvanic current measurements: six plates of magnesium and six plates of steel. Each of the metal plates had the following dimensions: 1.2 mm thickness  $\times$  35 mm width, with 42 mm<sup>2</sup> surface area exposed to the electrolyte. In Fig. 1(b) these plates are numbered 1–6 for both the AZ91D plates and the steel plates, with the numbers increasing as the plates are further from the AZ91D–steel interface. To ensure that plates 5 and 6 were able to provide current measurements at a sufficient distance from the AZ91D–steel interface, an extra plate of considerable thickness was added between plates 4 and 5, and also between plates 5 and 6. Moreover, to ensure there were no end effects for the AZ91D plate 6, there was an additional AZ91D plate molded after AZ91D plate 6.

This GCA allowed investigation of various anode/cathode ratios and different insulation spacing between the AZ91D and steel by appropriate electrical connections of the plates.

The GCA was designed with the connections as shown in Fig. 1(b) to allow measurement of the galvanic current density distribution for an “infinite” plate of AZ91D coupled to a finite plate of steel as an idealization of a large plate of AZ91D adjacent to a small plate of steel. The configuration was chosen to maximize the extent of the current density distribution that could be measured for the AZ91D side of the couple, that is, the current density in the AZ91D plate 6 should be small compared with the current density in AZ91D plate 1. The plates 1–6 for AZ91D and steel were arranged in a symmetrical pattern with respect to the AZ91D–steel interface. The current density distribution was plotted (see Fig. 7) in terms of the actual distance (in cm) from AZ91D plate 6, so that the AZ91D–steel interface was at a distance  $D = 2$  cm.

For these connections, the area ratio of anode/cathode was designated as 1:1 as the current density measurement extended for 2 cm over AZ91D from AZ91D plate 1 to AZ91D plate 6, and likewise the current density measurement extended for 2 cm over the steel from steel plate 1 to steel plate 6. A larger area ratio of anode/cathode, designated as 2:1, was effected by removing the electrical connections to steel electrode 5, steel electrode 6 and the steel electrode between these two. The current density measurement extended for 2 cm over AZ91D from AZ91D plate 1 to AZ91D plate 6, and only for about 1 cm over the steel from steel plate 1 to steel plate 4. The current density distribution was again plotted (see Fig. 6) in terms of the actual distance (in cm) from AZ91D plate 6, so that the

AZ91D–steel interface was at a distance  $D = 2$  cm. A smaller area ratio of anode/cathode, designated as 1:2, was effected by keeping the electrical connections to all the steel electrodes as in Fig. 1(b) and removing the electrical connections to AZ91D electrode 5, AZ91 electrode 6 and the AZ91D electrodes between these two and after AZ91D electrode 6. The current density measurement extended for about 1 cm over AZ91D from AZ91D plate 1 to AZ91D plate 4, and for 2 cm over the steel from steel plate 1 to steel plate 6. The current density distribution was plotted (see Fig. 8) with the AZ91D–steel interface at a distance  $D = 1$  cm, with the measurements from AZ91D electrode 1 to AZ91D 4 on the left hand side of the figure, and steel electrode 1 to steel electrode 6 on the right hand side and extending over 2 cm.

The influence of solution depth was studied using the arrangement as shown in Fig. 1(b) (this has a solution depth  $d = 10$  mm), and with a solution depth of  $d = 1$  mm (Fig. 9) and  $d = 3$  mm (Fig. 10).

With the connections shown in Fig. 1(b), the AZ91D–steel galvanic couple has an insulating distance  $s = 0.5$  mm. An insulating distance  $s = 2.2$  mm can be effected by removing the electrical connection to either AZ91D plate 1 or steel plate 1 and to cover the plate with epoxy resin.  $s = 3.9$  mm can be effected by removing the electrical connection to both AZ91D plate 1 and steel plate 1 and to cover these plates with epoxy resin. Similarly,  $s = 7.3$  mm, 10.7 mm, ... can be effected by removing extra electrical connections and to cover these plates with epoxy resin. This approach allows study of the influence of insulating distance between the anode and cathode. Inherent in this approach is that the area of anode and cathode decreases as the insulating distance is increased.

## 2.2. Galvanic interaction assembly

The galvanic interaction assembly (GIA) was designed to allow investigation of the manner of interaction of two (independent) galvanic couples. A section through the GIA is shown schematically in Fig. 2. The GIA consisted of a steel–AZ91D–steel arrangement (designated as St\_Mg\_St), with current measurement as for the GCA. The arrangement was symmetrical, so the extent of the steel was identical on both sides of the central AZ91D. Furthermore, there was similar flexibility in making electrical connections. The concept was that the AZ91D would experience current from two identical galvanic couples, namely there was (1) the left hand side galvanic couple: St\_Mg, and (2) the right hand side galvanic couple: Mg\_St. Furthermore, the left hand galvanic couple, St\_Mg was identical to the right hand galvanic couple Mg\_St. The GIA allowed measurement of the current density distribution for the full interaction situation, namely steel–AZ91D–steel, and moreover, allowed independent measurement of the two independent galvanic couples: (1) St\_Mg and (2) Mg\_St. This allowed investigation of the kind of interaction law that would describe how the current density for the case of the two interacting identical galvanic couples was combined from the individual galvanic couples.

The GIA consisted of 12 mild steel plates and 6 AZ91D plates as shown in Fig. 2. The surface area of each plate exposed to the electrolyte was  $56 \text{ mm}^2$  for each steel plate with 1.6 mm (thickness)  $\times$  35 mm (width) and  $42 \text{ mm}^2$  for each AZ91D plate with 1.2 mm (thickness)  $\times$  35 mm (width). The connections for the measurement of the galvanic current for the GIA could be made connecting all the plates as shown Fig. 2. This arrangement is designated St\_Mg\_St, and allows the measurement of the interaction of the galvanic corrosion from the galvanic couple on the left (i.e. St\_Mg) and from the galvanic couple on

the right side (i.e. Mg\_St). The current density was plotted against distance from the left hand steel electrode 1, as shown in Fig. 11. This same convention was used throughout when presenting the current density for the GIA regardless of the details of the electrical connections. This convention was adopted to facilitate comparison between the plots.

There are 18 connections for the arrangement with all electrodes connected as illustrated in Fig. 2, however the ZRA had only 12 channels, so that only 12 currents could be measured simultaneously. The measuring procedure adopted was to measure the currents from the 12 electrodes from the left, or the 12 electrodes from the right. A total of five tests were carried out as shown in Fig. 11.

In addition to the arrangement with all electrodes connected as illustrated in Fig. 2, the electrical connections could also be made to separately measure the galvanic currents from the left hand side couple (St\_Mg) or alternatively separately measure the galvanic currents associated with the right hand side couple (Mg\_St). For these measurements, there were no electrical connections to the six right hand side electrodes (RHS steel electrodes 1–6) for the St\_Mg couple; or alternatively there were no electrical connections for the left steel electrodes 1–6 for the Mg\_St couple. In each case, all currents could be measured simultaneously as there were 12 electrodes and also 12 channels for the ZRA. The data was plotted as shown in Fig. 12, using the same convention as for Fig. 11.

### 2.3. Electrolyte

5% NaCl solution was used because it represents a severe corrosive environment and there was good agreement between the BEM calculation and the experimental measurement in our previous study [15]. The galvanic current was quite stable with little corrosion product interference and thus it is much easier to distinguish the effect of geometry from other factors such as a corrosion product film. The 5% NaCl solution was made with analytical reagents and deionized water. The conductivity was measured using a platinum conductivity cell to be 79,500  $\mu\text{S cm}$ . The solution depth was arbitrarily set at  $d = 10$  mm except for the experiments which specifically studied the influence of the solution depth,  $d$ .

### 2.4. Galvanic current density measurement procedure

The surface of the electrodes of the GCA or GIA was polished using 1200# silicon carbide abrasive paper, washed with water and ethanol, and dried. The assembly was immediately immersed in the solution. A multi-channel zero resistance ammeter (ZRA) was used to measure the galvanic current passing through each electrode as a function of time as illustrated in Figs. 1(b) and 2. The current density was calculated by dividing the measured current by the area of the electrode.

### 2.5. Polarization curve measurement

Fig. 3 presents the experimental arrangement for measurement of the polarization curves. Separate specimens were made for AZ91D and steel. Potentiodynamic and galvanostatic polarization curves were measured. The potentiodynamic curves gave a guide for the applied current density values for the measurement of the galvanostatic polarization curves. For each applied constant current density, the potential was measured with time; (details are given in our prior work [15]). The galvanostatic polarization curves were

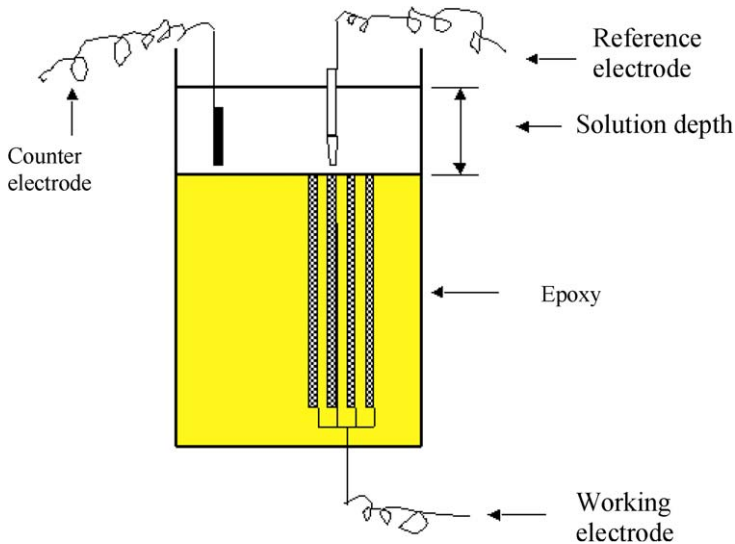


Fig. 3. Schematic arrangement for measuring the polarization curves. Separate specimens were made for AZ91D and for steel.

obtained by plotting the measured potential versus applied current density at 5–10 min as illustrated in Fig. 4 [15]. For each curve, multiple measurements were made. Three typical potentiostatic polarization curves are defined by the values given in Table 1. These curves were used as the boundary conditions for the BEM model. Three typical measured polarization curves were used in order to evaluate the influence of typical errors in the measurement of the polarization curves. The 1287 electrochemical interface was used to measure the polarization curves. An Ag/AgCl reference electrode was used. The solution resistance was measured using the 1255B Frequency Response Analyzer before the start of each test.

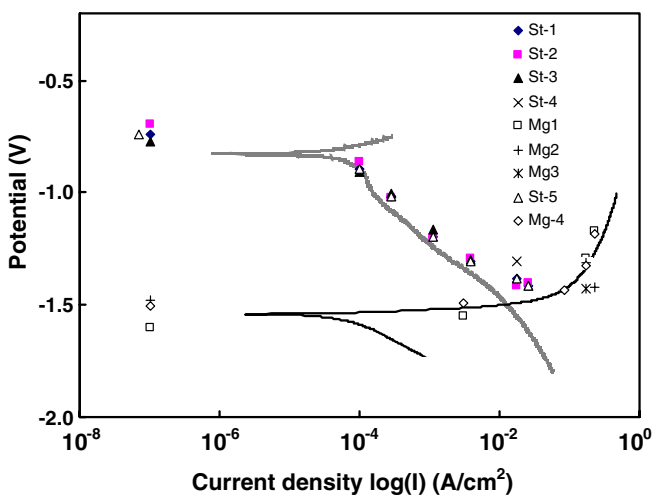


Fig. 4. Galvanostatic polarization curve measurements (data points) in 5% NaCl solution. Curves represent typical potentiodynamic polarization curves, at a scan rate of 2 mV/s. An Ag/AgCl reference electrode was used.

Table 1  
Boundary conditions in 5% NaCl solution

Current density (mA/cm <sup>2</sup> )	Potential (V)		
	BEM 1	BEM 2	BEM 3
<i>Steel</i>			
0.000	-0.771	-0.695	-0.741
0.100	-0.906	-0.863	-0.896
0.290	-1.003	-1.021	-1.018
1.100	-1.165	-1.202	-1.194
3.860	-1.298	-1.296	-1.305
17.700	-1.307	-1.413	-1.386
25.400	-1.418	-1.403	-1.417
<i>AZ91D</i>			
0.000	-1.480	-1.600	-1.506
-3.058	-1.430	-1.550	-1.492
-84.880	-1.431	-1.431	-1.431
-172.500	-1.310	-1.290	-1.325
-230.100	-1.420	-1.170	-1.183

The polarization curves were corrected for the potential drop caused by the solution resistance.

### 3. BEM model

The mathematical formulation has been presented by Adey and Niku [17] for a uniform, isotropic electrolyte domain  $\Omega$  as illustrated in Fig. 5. For a uniform, isotropic electrolyte system in steady state, the potential obeys the Laplace equation:

$$\nabla^2 \phi = 0, \tag{1}$$

The Laplace equation is solved using the following boundary conditions:

$$\phi = \phi_0, \quad \text{on } \Gamma_1, \tag{2}$$

$$I = I_0, \quad \text{on } \Gamma_2, \tag{3}$$

$$I_a = -f_a(\phi), \quad \text{on } \Gamma_{3a}, \tag{4}$$

$$I_c = -f_c(\phi), \quad \text{on } \Gamma_{3c}, \tag{5}$$

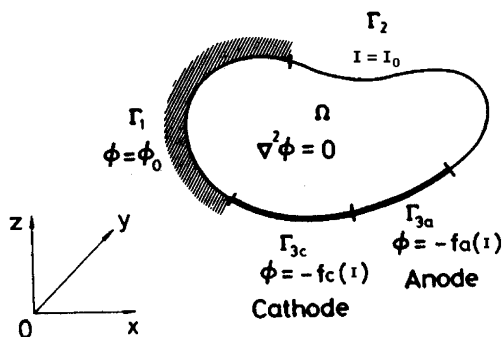


Fig. 5. Basic equations and boundary conditions for the BEM.

where  $\Gamma (\equiv \Gamma_1 + \Gamma_2 + \Gamma_{3a} + \Gamma_{3c})$  is the entire surface of the electrolyte domain  $\Omega$ ,  $I$  is the current density across the boundary, and  $\phi$  is the potential.  $\phi_0$  and  $I_0$  are given constant values of potential and current density respectively. For the current research, there was no region  $\Gamma_1$  of applied potential, and  $I = 0$  applied for all regions other than the AZ91D and steel electrodes in Figs. 1(b) and 2.  $f_a(\phi)$  and  $f_c(\phi)$  are linear or non-linear functions that describe the anode and cathode electrode kinetics respectively.

The boundary integral equations for all elements can be assembled into a system of linear simultaneous equations, which is expressed in a matrix form as follows:

$$H\phi = GI \quad [17], \quad (6)$$

where  $H$  and  $G$  are problem influence matrices, and  $\phi$  and  $I$  represent potential and current density vectors respectively. The size of the equation system is defined by the number of nodes. Partitioning the  $\phi$  and  $I$  into those nodes which form the anode and the cathode regions and applying the boundary condition of Eqs. (4) and (5), gives

$$\begin{bmatrix} h_{aa} & h_{ac} \\ h_{ca} & h_{cc} \end{bmatrix} \begin{bmatrix} \phi_a \\ \phi_c \end{bmatrix} = \begin{bmatrix} g_{aa} & g_{ac} \\ g_{ca} & g_{cc} \end{bmatrix} \begin{bmatrix} f_a(\phi_a) \\ f_c(\phi_c) \end{bmatrix} \quad [17], \quad (7)$$

where  $\begin{bmatrix} h_{aa} & h_{ac} \\ h_{ca} & h_{cc} \end{bmatrix}$  and  $\begin{bmatrix} g_{aa} & g_{ac} \\ g_{ca} & g_{cc} \end{bmatrix}$  are elements of the problem influence matrices,  $\begin{bmatrix} \phi_a \\ \phi_c \end{bmatrix}$  and  $\begin{bmatrix} f_a(\phi_a) \\ f_c(\phi_c) \end{bmatrix}$  are the polarization curves. Eq. (7) was then solved by the iterative method, the Newton–Raphson method.

In this study, the non-linear relationships between potential and current density Eqs. (4) and (5) were determined as the experimentally measured polarization curves for the AZ91D and steel elements. The geometry of the galvanic couple of AZ91D–steel was created in BEASY environment corresponding to the real galvanic couples as illustrated in Figs. 1(b) and 2. A gradient of increasingly fine mesh size towards the AZ91D and steel interface was used where a sharp potential gradient was expected. Otherwise, the mesh size of electrolyte elements were evenly divided to reduce the element number.

The input parameters for the BEASY BEM model included the physical geometry of the galvanic couple, the electrolyte conductivity and the boundary conditions of  $\begin{bmatrix} \phi_{a0} \\ \phi_{c0} \end{bmatrix}$  and  $\begin{bmatrix} f'_a(\phi) \\ f'_c(\phi) \end{bmatrix}$ , where  $\phi_{a0}$  was the open circuit potential of the anode;  $\phi_{c0}$  was the open circuit potential of the cathode;  $f'_a(\phi)$  was the function used in BEASY to represent the anode metal polarization curve given by Eq. (4); similarly  $f'_c(\phi)$  is the function representing the cathode metal polarization curve. The functions  $f'_a(\phi)$  and  $f'_c(\phi)$  were defined using the piecewise linear approach using the values given in Table 1. The polarization curve was divided into small segments, such that for each segment, there was a linear relationship between the potential and current given by

$$I = f(\phi) = k(\phi - \phi_a) + I_a, \quad (8)$$

where  $k$ ,  $\phi_a$  and  $I_a$  were constants for each line segment.

## 4. Results

### 4.1. Effect of area ratio of anode/cathode

Figs. 6–8 illustrate the galvanic current density distribution for the AZ91D–steel galvanic couple in 5% NaCl solution for various area ratios of anode/cathode. (The galvanic current density was measured over a time span of 55 min [15], sufficient to ensure steady state, and steady state current density values are used throughout this paper.) The current density distributions from the BEM model are compared with the

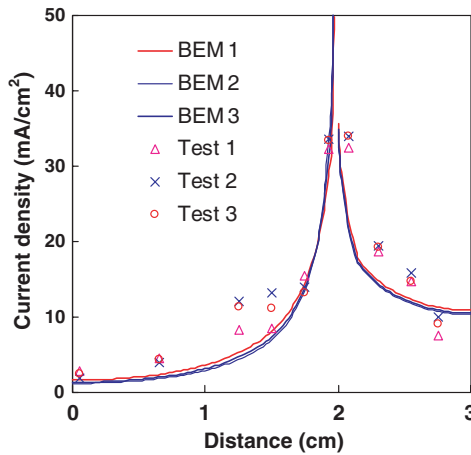


Fig. 6. Comparison of BEM model (curves) and experiment data (data points) for an area ratio of  $A/C$  of 2:1,  $d = 10$  mm.

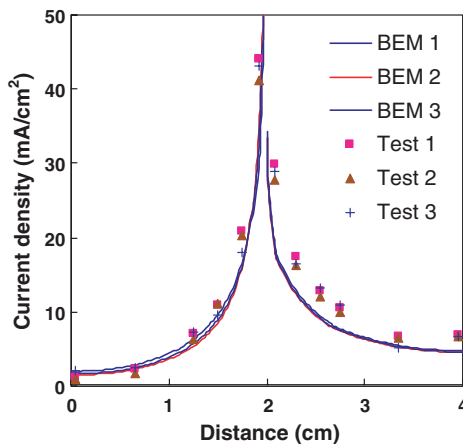


Fig. 7. Comparison of galvanic current density distribution between the BEM model (curves) and experiment data (data points) for an area ratio of  $A/C$  of 1:1,  $d = 10$  mm.

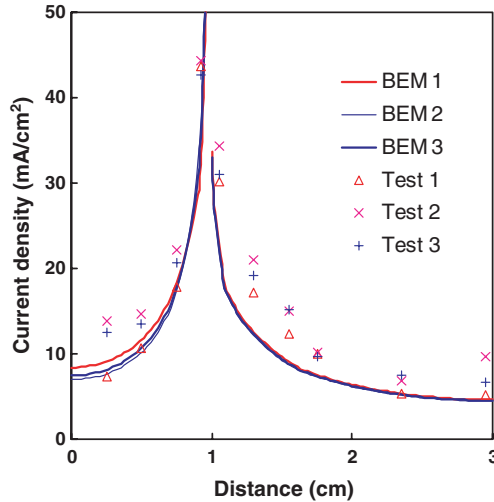


Fig. 8. Comparison of galvanic current density distribution between the BEM model (curves) and experiment data (data points) for an area ratio of  $A/C$  of 1:2,  $d = 10$  mm.

experimental measurement for an area ratio of anode/cathode of 2:1 in Fig. 6, of 1:1 in Fig. 7 and of 1:2 in Fig. 8. The BEM model used the three boundary conditions as given in Table 1. These are the three curves designated BEM 1, BEM 2 and BEM 3. The results of three independent experimental measurements are plotted as the data points and labeled Test 1, Test 2 and Test 3. There was good agreement between the BEM model and the experimental measurements.

The galvanic current density of the AZ91D electrode increased (as the area ratio was decreased from 2:1 to 1:2) from  $33 \text{ mA/cm}^2$  to  $44 \text{ mA/cm}^2$  for electrode Mg 1 (closest to the AZ91D–steel interface), from  $14 \text{ mA/cm}^2$  to  $22 \text{ mA/cm}^2$  for electrode Mg 2, from  $11 \text{ mA/cm}^2$  to  $17 \text{ mA/cm}^2$  for electrode Mg 3 and from  $10 \text{ mA/cm}^2$  to  $14 \text{ mA/cm}^2$  for electrode Mg 4. The galvanic current density of the AZ91D electrodes increased with the decrease of area ratio of anode/cathode as expected both experimentally and theoretically from prior study [3]. The influence of area ratio of anode/cathode on the galvanic current density distribution for AZ91D–steel in 5% could be reasonably predicted using the BEM approach.

#### 4.2. Influence of solution film depth, $d$

Figs. 7, 9 and 10 present the galvanic current density distributions from the BEM model compared with the experimental measurements for solution film depth values of 10 mm, 1 mm and 3 mm respectively. The BEM models were calculated using the three different boundary conditions as presented in Table 1. The galvanic current density of each electrode increased with the increase of solution film depth as expected because the increase of the solution film depth resulted in a larger area for the current to pass and thus reduced the resistance against the current flow. There was reasonable agreement both in trend and in current density value between the BEM model and the experimental measurement. Again the scatter in the experimental measurement of the galvanic current density was

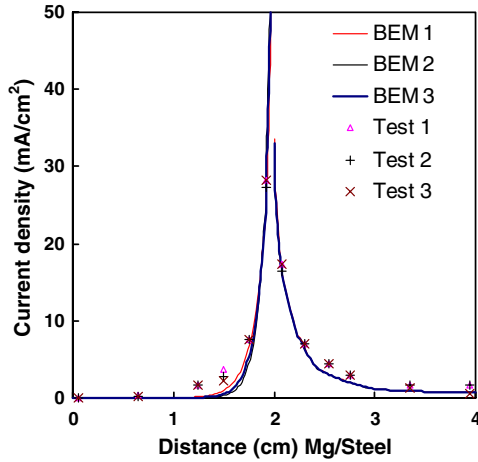


Fig. 9. Comparison of galvanic current density distribution between the BEM model (curves) and experimental measurements (data points),  $d = 1$  mm.

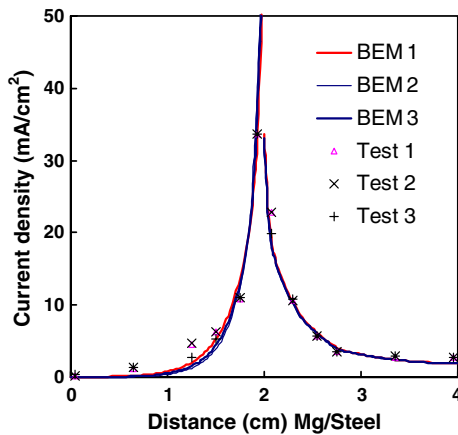


Fig. 10. Comparison of galvanic current density distribution between the BEM model (curves) and experimental measurements (data points),  $d = 3$  mm.

comparable or greater to the scatter in the BEM curves. The scatter in Figs. 9 and 10 was less than in Figs. 6–8; the lower scatter was attributed to the lower current density values in Figs. 9 and 10.

#### 4.3. Galvanic corrosion interaction

Fig. 11 presents the galvanic current density distribution for both the BEM model and the experimental measurements for the whole galvanic corrosion interaction assembly, Fig. 2, i.e. for the St\_Mg\_St configuration. Only one curve has been shown, that corresponding to the typical boundary condition BEM 2, since the previous calculations (Figs. 6–10) had indicated only a small amount of scatter arising from the errors in measurement

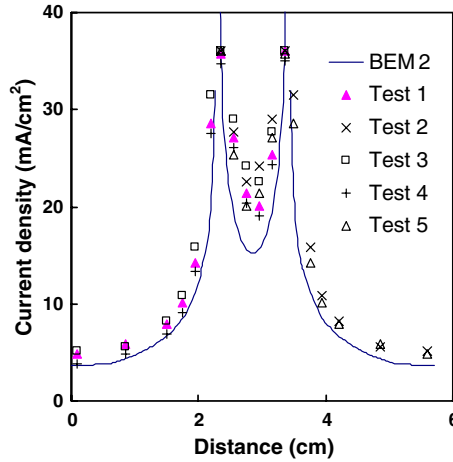


Fig. 11. Comparison between the BEM model (curves) and the experimental measurements (data points) of the galvanic current density distribution for the galvanic corrosion interaction assembly (St\_Mg\_St) as illustrated in Fig. 2,  $d = 10$  mm.

of the polarization curves. There was a good agreement between the BEM model and the experimentally measured values.

Fig. 12 presents both (a) the galvanic current density distribution for the steel–AZ91D galvanic couple (curve St\_Mg) without any galvanic interaction, and also (b) the AZ91D–

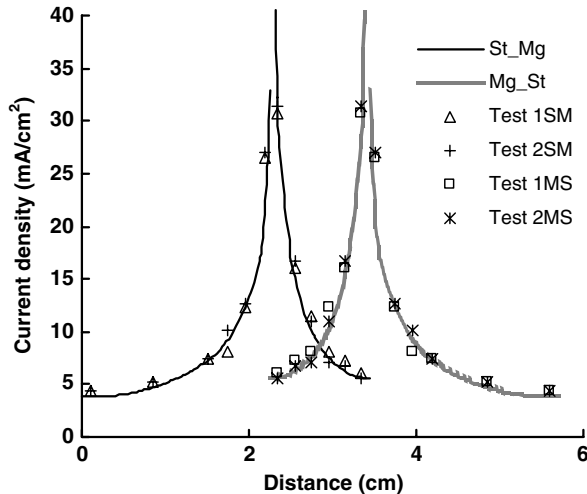


Fig. 12. Comparison between the BEM model (curves) and the experimental measurements (data points) of the galvanic current density distribution without galvanic interaction. Separate calculations and experimental measurements were first made for the Steel–Mg couple (i.e. connecting only the six steel and the six AZ91D plates on the left of the galvanic corrosion interaction assembly illustrated in Fig. 2 to give the curve St\_Mg and the data (Test 1SM and Test 2SM). Subsequently calculations and experimental measurements were made for Mg\_St by connecting the six AZ91D plates to the six steel plates on the right.  $d = 10$  mm.

steel galvanic couple (curve Mg\_St) without any galvanic interaction. There was a good agreement between the BEM model and the experimental measurements for both cases (a) and (b).

Fig. 13 presents the curve “Addition” as the linear addition of the galvanic current density for the AZ91D electrodes calculated for steel–AZ91D couple and AZ91D–steel couple, without galvanic interaction. The superimposed galvanic current density for the AZ91D electrodes was in good agreement with the BEM model for the steel–AZ91D–steel galvanic interaction assembly.

Fig. 14 presents the addition of the measured galvanic current density for the AZ91D electrode measured for the steel–AZ91D couple and for the AZ91D–steel couple, without galvanic interaction. Fig. 14 also has the curve “Addition” from Fig. 13 and the curve St\_Mg\_St from Fig. 11. There was good agreement between the linear addition of the experimental measurements and BEM calculations. This indicated that the current density distribution for the AZ91D electrodes for galvanic interaction could be expressed approximately as a linear superposition of the current density caused by each individual galvanic couple.

#### 4.4. Effect of insulation distance, $s$

The prior sections have shown that the BEASY BEM program gave calculated values in good agreement with the experimental measurements. As a consequence, the BEASY BEM program was used to model the GCA to calculate the galvanic current density distribution for the AZ91D–steel galvanic couple in 5% NaCl solution for the insulation distance  $s = 0.5$  mm, 2.2 mm, 3.9 mm, 7.3 mm, 10.7 mm and 25 mm. Fig. 15 presents the calculated galvanic current density distribution for each case. It is useful to use the symbol  $n$  to designate the general curve;  $n$  has the values 1, 2, 3, 4, 5 and 6. This approach allowed

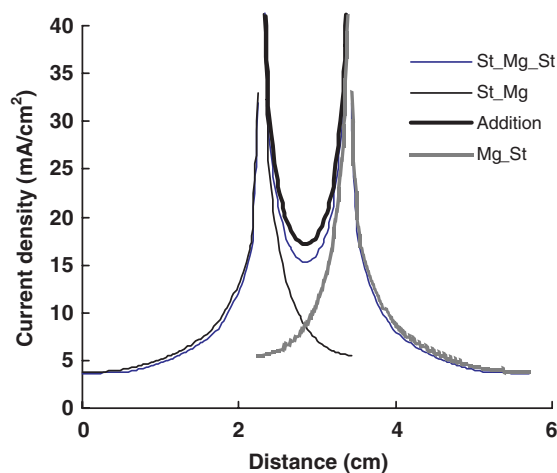


Fig. 13. Comparison of the BEM model for the non-interacting galvanic current density distributions (St\_Mg and Mg\_St), the interacting galvanic current density distribution (St\_Mg\_St) and the linear addition of the non-interacting galvanic current density distributions (curve “Addition”).

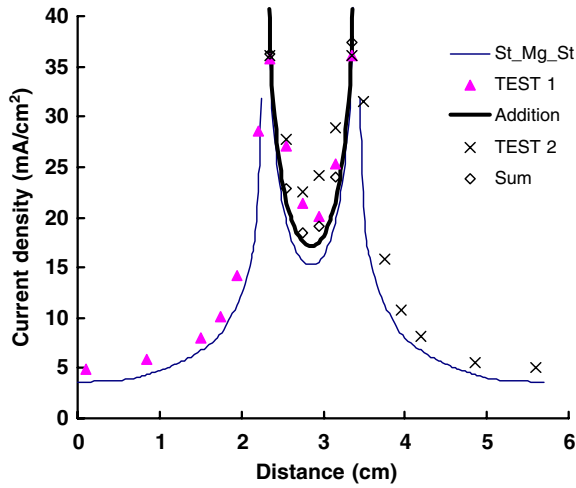


Fig. 14. Comparison of superposition of the non-interacting galvanic current density distribution (curve “Addition”), the interacting galvanic current density distribution (curve “St\_Mg\_St”), measured interacting galvanic current density distributions (data points from the Fig. 11) and linear addition of the measured non-interacting galvanic current density distributions (data points designated as “Sum”).

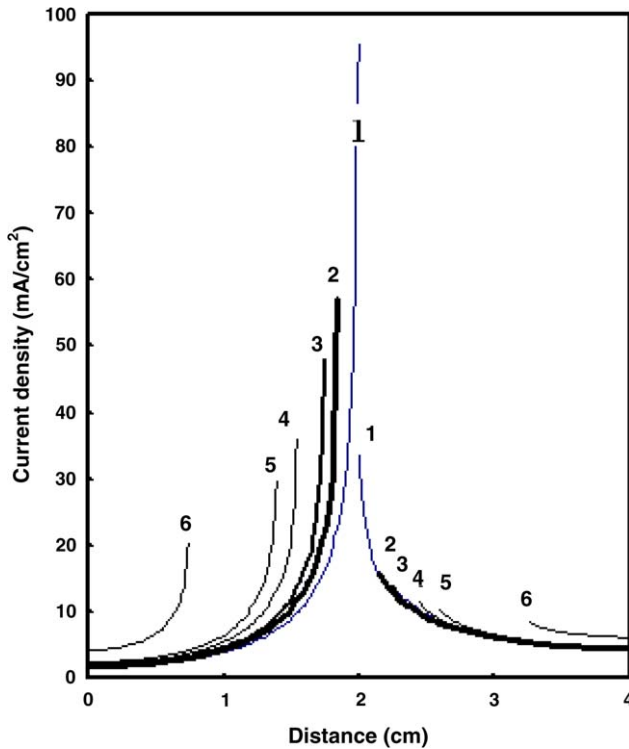


Fig. 15. The galvanic current density distribution calculated using the BEASY BEM model for the following values of the insulation distance,  $s = 0.5$  mm (curve 1),  $s = 2.2$  mm (curve 2),  $s = 3.9$  mm (curve 3),  $s = 7.3$  mm (curve 4),  $s = 10.7$  mm (curve 5) and  $s = 25$  mm (curve 6).

study of the influence of insulating distance between the anode and cathode. It was possible to obtain the following: (1) the current density distributions, presented in Fig. 15, (2) the maximum galvanic current density for the AZ91D electrode immediately adjacent to the steel, presented in Fig. 16, (3) the total galvanic current  $I_T(n)$  and (4) the average galvanic current density  $I_a$ . The total galvanic current was equal to the integration of the current density values over the area  $A(n)$  of each current density distribution. The average galvanic current was equal to  $I_T(n)/A(n)$ .

The galvanic current density of the AZ91D electrodes decreased as the insulating distance increased, Fig. 15. Furthermore, the maximum galvanic current density for the AZ91D electrode adjacent to the steel decreased significantly with the increase of the

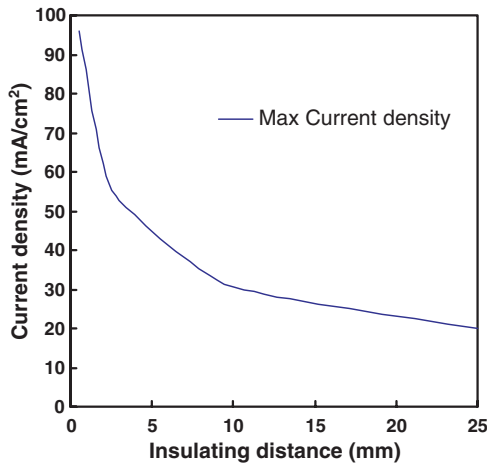


Fig. 16. Maximum galvanic current density versus insulating distance, s.

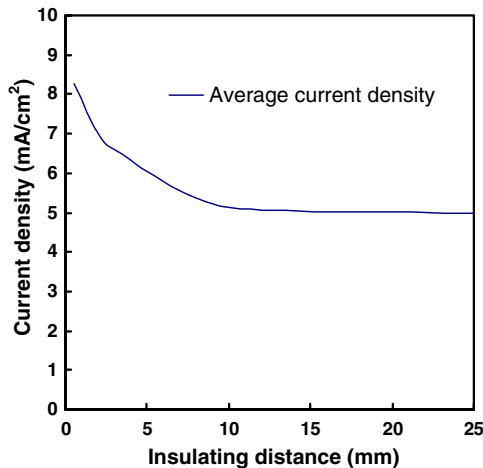


Fig. 17. Average galvanic current density versus insulating distance.

insulating distance (Fig. 16). Moreover, the total galvanic current for AZ91D electrodes also decreased as the insulating distance increased. Interpretation of the significance of the total current is difficult because two variables had been changed simultaneously: the area was decreased at the same time as the insulating distance was increased. Fig. 17 shows that the average current density decreased with increasing insulating distance.

In another words, the increase of insulating distance leads to less galvanic corrosion attack both locally and on average. The influence of the insulating distance on the galvanic current distribution of steel electrodes were the same as that on the AZ91D electrodes. However, the magnitude of the influence on the steel electrodes was much smaller than that on the AZ91D electrodes. This BEM simulation was within expectations. It is also consistent with the results and the theoretical predictions of Song et al. [3]. The increase of the insulating distance increases the length of the circuit and thus increases the resistance of the circuit. Therefore the galvanic current density of the adjacent anode and cathode decreases according to Ohm's law.

## 5. Discussion

### 5.1. Steady state

The measurements of the polarization curves were carried out in a potentiostatic manner. For each data point for each curve, a constant current was applied, and the potential was measured. Care was taken to ensure that steady state had been reached, so that the measured potentiostatic curves represented steady state conditions [15]. Similarly, for the measurement of galvanic current density using the GCA and the GIA, care was taken to ensure that the galvanic current density measurements represented steady state conditions [15]. This meant that it was valid to compare the experimental measured galvanic current density with the predictions of the BEM model because both were for steady state conditions, and were thus directly comparable. The fact that there was good agreement between the experimental measurements and the BEM calculations provides assurance that the approach is sound to use the GCA and the GIA to measure galvanic current density distributions.

### 5.2. Influence of experimental error

Figs. 6–10 illustrate the galvanic current density distribution for the AZ91D–steel galvanic couple in 5% NaCl solution for various area ratios of anode/cathode and solution depth. The current density distributions from the BEM model are compared with the experimental measurement. The BEM model used the three boundary conditions as given in Table 1. These are the three curves designated BEM 1, BEM 2 and BEM 3. The results of the three independent experimental measurements are plotted as the data points and labeled Test 1, Test 2 and Test 3. There was good agreement between the BEM model and the experimental measurements.

The influence of the experimental error in the measurement of each polarization curve as input to the BEM model meant that the BEM model gave three different curves, which had slightly different values. Similarly, there was experimental scatter in the experimental measurement of the current density for each metal plate of the GCA. Figs. 6–10 indicated that the directly measured galvanic current density had an experimental scatter larger than

the differences in the BEM curves caused by the scatter in the measurements of the polarization curves.

### 5.3. Experimental approach

Figs. 6–12 indicated in each case that there was good agreement between the BEM model and the experimental measurement of the current density. The experimental measurements corresponded to measurements at discrete positions from individual metal plates that were separated from each other by an insulation material 0.5 mm in thickness. In comparison, the BEM model was for a continuous electrode with no interruptions due to insulating spacers. The agreement between the BEM model and the experimental measurements indicated that the GCA and GIA provide sound methodologies for the measurements of galvanic current density distributions, and that the BEM model provided good predictions of the galvanic current density distribution.

### 5.4. Influence of area of anode/cathode

The galvanic current density of the AZ91D electrodes increased with the decrease of area ratio of anode/cathode. This result is consistent with expectations from basic corrosion theory. As the area ratio of anode/cathode increases, there is available a higher relative cathodic current density. Since the anode current equals the cathode current, the anode current density increases.

### 5.5. Galvanic corrosion interaction

The experimental measurements and the BEM modeling involving the GIA indicated that the current density distribution for the AZ91D electrodes for galvanic interaction could be expressed approximately as a linear superposition of the current density caused by each individual galvanic couple. At first blush, this is a somewhat surprising outcome because the boundary conditions are very non-linear as is clear from Fig. 4.

### 5.6. Effect of insulation distance, $s$

Because the BEASY BEM program gave calculated values in good agreement with the experimental measurements, the BEASY BEM program was used to model the GCA to study the influence of insulating distance. Inherent in this approach was that the area of the anode and cathode decreased as the insulating distance was increased. Future work proposes to study the increase of insulating distance whilst keeping constant the areas of anode and cathode.

### 5.7. Implication and applicability to service and future research

The galvanic current density of the AZ91D electrodes decreased as the insulating distance increased. The increase of the insulating distance increases the length of the circuit and thus increases the resistance of the circuit. Therefore the galvanic current density of the adjacent anode and cathode decreases according to Ohm's law. It has been suggested that these results could be used to produce simple empirical formulations that can be used

to provide rough estimates for service conditions. However, it is thought that a much better way forward is the development of a user-friendly BEM package that could be used as a design tool to give quantitative evaluations of the galvanic current density distribution associated with a particular design. The research presented herein and our prior research on galvanic corrosion [14–16] give confidence that such a BEM package is indeed possible. However, additional research is needed to address the following points:

- Influence of thin solution films. It is conceivable that, for very thin surface solution films, the corrosion process for Mg can be different to that in a bulk solution [1,2]. In particular, oxygen reduction may become an important cathodic reaction. Local alkalization in the thin solution film would be expected to facilitate formation of a partially protective film. These considerations are of particular importance when considering a realistic exposure of auto components to salt spray. Thin solution films and high solution surface area can imply high availability of oxygen for the cathodic reaction.
- Influence of the composition of the surface solution film. Use of a 5% NaCl solution has been found to give BEM predictions in good agreement with experimental measurements. This solution represents an aggressive environment, and is realistic for service conditions in North America or Europe where there is significant de-icing salt usage and there is consequently an issue from the resulting salt spray. A sodium chloride solution could also be considered as providing a simple analogue to marine exposure. Moreover, the NaCl solution will provide a “worst case” situation. If a design can be formulated to provide adequate performance in a NaCl solution, then it would be expected to perform better in a less aggressive environment. Nevertheless, it is important to have an adequate approach to less aggressive environments as Mg is widely used in environments much less aggressive than salt spray.
- Understanding of self-corrosion [16], influence of the form of corrosion [18] (including in particular pitting corrosion), influence of the Mg Alloy (composition and microstructure) [18,19], and the negative difference effect [1,2,20,21].
- Influences of surface topography. So far our research has largely addressed 1D galvanic corrosion. Ahead is the challenge of 2D influences.
- What are the effects due inclination of the magnesium surface?

## 6. Conclusions

The galvanic corrosion assembly (GCA) and galvanic interaction assembly (GIA) provide sound methodologies for the measurements of galvanic current density distributions.

The BEM based BEASY program can reasonably predict the galvanic current density distribution for AZ91D–steel in 5% NaCl solution.

The directly measured galvanic current density had an experimental scatter larger than the differences in the BEM curves caused by the scatter in the measurements of the polarization curves.

The galvanic current density of the AZ91D electrodes increased with the decrease of area ratio of anode/cathode.

The galvanic current density of each electrode increased with the increase of solution film depth as expected because the increase of the solution film depth resulted in a larger area for the current to pass and thus reduced the resistance against the current flow.

The galvanic current density of the AZ91D electrodes decreased as the insulating distance increased. The maximum galvanic current density for the AZ91D electrode adjacent to the steel decreased significantly with the increase of the insulating distance. Furthermore, the average galvanic current for AZ91D electrodes decreased as the insulating distance increased. In another words, the increase of insulating distance leads to less galvanic corrosion attack both locally and on average over the distribution.

The galvanic current density distribution on AZ91D electrodes caused by galvanic interaction can be reasonably predicted as the linear superimposition of current of caused by each individual galvanic couple.

## Acknowledgements

The authors would like to acknowledge the support of the Cooperative Research Centre for Cast Metals Manufacturing (CAST). CAST was established and is funded in part by the Australian Government's Cooperative Research Centres Program.

## References

- [1] G. Song, A. Atrens, *Advanced Engineering Materials* 5 (2003) 837.
- [2] G. Song, A. Atrens, *Advanced Engineering Materials* 1 (1999) 11.
- [3] G. Song, B. Johannesson, S. Hapugoda, D. St. John, *Corrosion Science* 46 (2004) 955.
- [4] G. Song, D. St. John, C. Bettle, G. Dunlop, *JOM* 57 (2005) 54.
- [5] G. Song, D. St. John, *Materials and Corrosion* 56 (2005) 15.
- [6] H.P. Hack, in: R. Baboian (Ed.), *Corrosion Tests and Standards Application and Interpretation*, American Society for Testing and Materials, Fredericksburg, VA, 1995, p. 186.
- [7] J.T. Waber, *Corrosion* 13 (1957) 95t.
- [8] D.J. Astley, *ASTM Spec. Tech. Publ. 978, Galvanic Corrosion*, 1988, p. 53.
- [9] D.J. Astley, *Chemistry & Industry (London)* (13, Suppl., *Seawater Cool. Chem. Plant*) (1977) 4.
- [10] J.W. Fu, *ASTM Spec. Tech. Publ. 978, Galvanic Corrosion*, 1988, p. 79.
- [11] R.A. Adey, S.M. Niku, *ASTM Spec. Tech. Publ. 978, Galvanic Corrosion*, 1988, p. 96.
- [12] R.G. Kasper, E.M. Valeriotte, in: H.P. Hack (Ed.), *Galvanic Corrosion*, American Society for Testing and Material, Philadelphia, 1988.
- [13] H.P. Hack, *Corrosion Reviews* 15 (1997) 195.
- [14] J.X. Jia, G. Song, A. Atrens, *Materials and Corrosion* 55 (2004) 845.
- [15] J.X. Jia, G. Song, A. Atrens, *Materials and Corrosion* 56 (2005) 259.
- [16] J.X. Jia, A. Atrens, G. Song, T.H. Muster, *Materials and Corrosion* 56 (2005) 468.
- [17] R.A. Adey, S.M. Niku, *ASTM Spec. Tech. Publ. STP 1154, Computer Modeling in Corrosion*, 1992, p. 248.
- [18] G. Song, A. Atrens, X. Wu, B. Zhang, *Corrosion Science* 40 (1998) 1769.
- [19] G. Song, A. Atrens, M. Dargusch, *Corrosion Science* 41 (1999) 249.
- [20] G. Song, A. Atrens, D. St. John, J. Nairn, Y. Li, *Corrosion Science* 39 (1997) 855.
- [21] G. Song, A. Atrens, D. St. John, X. Wu, J. Nairn, *Corrosion Science* 39 (1997) 1981.